Master's Thesis of Engineering

Floor Determination Algorithm Using Shape Analysis of Heading Signal for Stair Walking in Pedestrian Navigation

보행자 항법에서 계단 보행 시 진행 방향 신호의 형상 분석을 통한 층 결정 알고리즘

February 2022

Graduate School of Engineering
Seoul National University
Aerospace Engineering Major

Dong Chan Song

Floor Determination Algorithm Using Shape Analysis of Heading Signal for Stair Walking in Pedestrian Navigation

Advised by Professor Chan Gook Park

Submitting a master's thesis of Engineering

December 2021

Graduate School of Engineering
Seoul National University
Aerospace Engineering Major

Dong Chan Song

Confirming the master's thesis written by
Dong Chan Song
December 2021

Chair _____(Seal)

Vice Chair _____(Seal)

Examiner _____(Seal)

Abstract

Floor Determination Algorithm Using Shape Analysis of Heading Signal for Stair Walking in Pedestrian Navigation

Dong Chan Song
Department of Aerospace Engineering
The Graduate School
Seoul National University

This master's thesis presents a new algorithm for determining floors in pedestrian navigation. In the proposed algorithm, the types of stairs are classified by shape analysis, and the floors are determined based on the stair type. In order to implement our algorithm, the walking direction estimated through the Pedestrian Dead Reckoning (PDR) system is used. The walking direction signal has different shapes depending on the stair types. Then, shape analysis is applied to the signal shapes of the walking direction to identify the types of stairs and determine the floor change. The proposed algorithm is verified through simulations and experiments, and it is confirmed that it works well even when moving through multiple floors with several different types of stairs. It is also verified that the performance is superior to the conventional floor determination algorithm.

Keywords: Pedestrian dead reckoning, Indoor navigation, Floor determination, Shape analysis, Shape distance, Classification

Student number: 2020-20377

Contents

List of Tables

List of Figures

Chapter 1

Introduction

1.1 Motivation and Background

Indoor navigation is needed in various fields such as military, fire-fighting, and civilian sectors. However, the Global Navigation Satellite System (GNSS) is not available indoors, and positioning is performed using only indoor equipment. So, various alternatives have been presented with additional sensors or methods [1].

Localization based on direct sensing tracks the position of a pedestrian by sensing identifiers or tags installed in the building [2]. These methods include RFID, IR (Infrared), Ultrasound, and Bluetooth. RFID stores and retrieves data using electromagnetic transmission to an RF-compatible integrated circuit [3]. The small RFID tags are beneficial when used in conjunction with many applications, but numerous types of infrastructure are required for accurate positioning [4]. IR uses transmitters installed in a known location, with a unique ID broadcast by each transmitter [5]. Ultrasound uses emitters installed in the infrastructure to broadcast ultrasound waves, and a receiver carried by a user receives these signals from the two closest emitters to determine his location [6]. The system is inexpensive and has a wide coverage area; however, it often experiences blocked or reflected signals or is affected by noise sources and low measurement accuracy [7]. Bluetooth is light and ubiquitous given its use in numerous devices, such as laptops, desktops, and

mobile phones [8]. Despite its advantages of reusability and low cost, its accuracy is low and sensitive to environmental changes [9].

The importance of 3D positioning for pedestrians is increasing, and related research is receiving much attention. Estimating height plays an important role because pedestrians change their floors when using stairs or elevators. Therefore, several studies related to height estimation are as follows: There are ways to utilize infrastructure inside buildings such as BLE, RFID, and Wi-Fi. However, there is a disadvantage in that it cannot be used without infrastructure or equipment to receive it. There is another way to use a barometer [12]. A barometer can calculate the height through an atmospheric pressure-height conversion equation using the lower atmospheric pressure as the height increases. However, indoor air pressure is not constant due to various factors such as heating and cooling equipment and changes in external air pressure. Next, the Weinberg method used in the step length estimation of PA is extended to 3D to calculate the height change when climbing stairs [13]. However, this method has a disadvantage because parameters should be tuned according to sensor position and each person. A research estimates height using a Kalman filter in PDR using a smartphone [14]. However, this method requires the help of a barometer and the specification of a barometer which is enough to distinguish at least one stair step.

1.2 Objectives and Contributions

After estimating the height using the method described above, the problem of determining the floors remains. Some studies use RFID [15], RSSI-fingerprint [16], and Wi-Fi [17] for floor determination but are only applicable to buildings equipped

with such infrastructure. These studies are also difficult to apply in emergencies without receivers. In addition, other studies propose new height estimation methods such as the Hidden Markov Model (HMM) [18] or PA-based method [19] with floor determination results, but experiments were conducted only on a simple type of stair. There is another conventional method of assuming the height of the floor. This method follows an algorithm that changes the number of the floor when the estimated height exceeds the threshold, the height of the floor. However, moving through multiple floors can miscalculate the floor if the actual floor height differs from the assumed floor height. In addition, errors can occur in buildings with floors that are not typical of floor height, such as the lobby.

Therefore, in this thesis, a new floor determination algorithm is proposed. The proposed algorithm has novelty in classifying stair types using the shape analysis of the pedestrian's walking direction signal. Furthermore, the effectiveness of the proposed algorithm is identified through simulation and experimental results, and the floor determination accuracy is also verified through multi-floor change experiment results.

This thesis is organized as follows. The next chapter explains the IA-based PDR system. Chapter 3 presents shape analysis to help understand the proposed algorithm. Chapter 4 describes the proposed algorithm, and Chapter 5 presents the results of its application to simulation and experimental data, respectively. Research summary and future work are given in the last chapter.

Chapter 2

Pedestrian Dead Reckoning System

2.1 Overview of Pedestrian Dead Reckoning

Localization based on the Pedestrian Dead Reckoning (PDR) system uses sensors attached to users to estimate their relative position based on a previous or known position. A benefit of the PDR is its low installation cost and lack of a requirement for additional sensors.

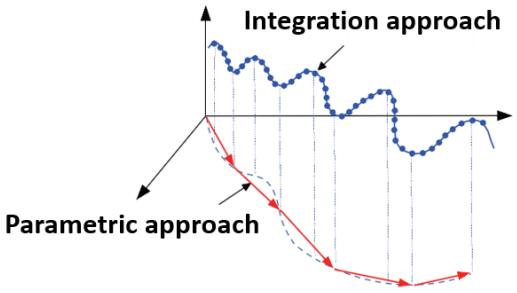

Figure 2.1: IA and PA-based PDR system

There are two methods in the PDR system: Integration Approach (IA) and Parametric Approach (PA), as shown in Figure 2.1. In IA, the IMU is attached to the shoe of the pedestrian. The accelerometer signal is double-integrated, and the gyroscope signal is integrated to calculate the position and attitude of the pedestrian like the Inertial Navigation System (INS) [10]. However, due to the accelerometer and gyroscope bias, estimating the position with pure INS gradually accumulates the position error. Therefore, IA uses the Extended Kalman Filter (EKF) with Zero

velocity UPdaTe (ZUPT) to correct estimation errors. Unlike IA, PA estimates the position of pedestrians by parametric method with step length and walking directions each time a step is detected [11]. In PA, the location of sensor attachment is relatively free compared to IA, but motion recognition algorithms are required because different parameters are applied to each sensor location.

2.2 Integration Approach

2.2.1 Strapdown inertial navigation system

Strapdown inertial navigation system (SDINS) is a type of navigation using inertial sensors. Using SDINS, real-time navigation solutions such as an object's position, velocity, and attitude can be obtained. An accelerometer and a gyroscope are attached to the object to measure the acceleration and angular velocity of the antibody. At this time, the accelerometer measures the specific force f^b defined as the non-gravitational force per unit mass. The block diagram of SDINS is shown in Figure 2.2.

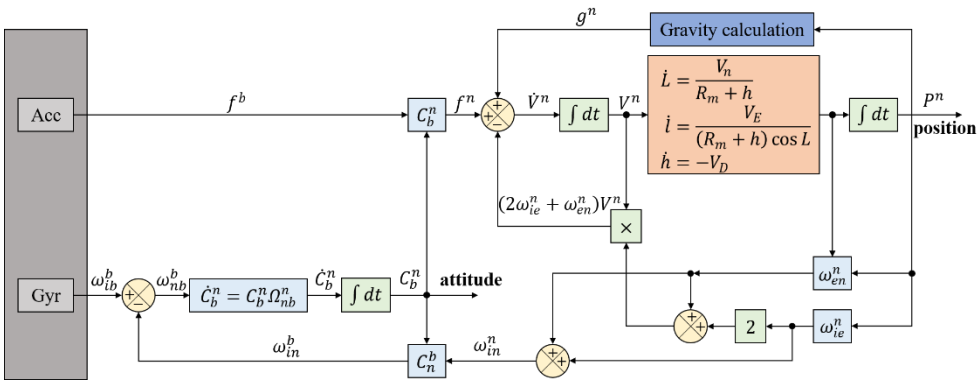

Figure 2.2: Block diagram of strapdown inertial navigation system

2.2.2 Extended Kalman filter

The Kalman filter is an optimal estimator for the state of a linear dynamic system disturbed by white noise. Unfortunately, most of the existing systems in nature are nonlinear systems. Therefore, there are some nonlinear estimators such as extended Kalman filter (EKF), unscented Kalman filter (UKF), particle filter (PF), etc. EKF is used in many studies because of its advantages of simple application and fast computational speed.

Assume the following nonlinear system:

$$\begin{aligned} x_k &= f_{k-1}(x_{k-1}, w_{k-1}) \\ y_k &= h_k(x_k, v_k) \\ w_k &\sim N(0, Q_k) \\ v_k &\sim N(0, R_k) \end{aligned} \tag{2.1}$$

Applying Taylor series expansion to linearize the system model is as follows:

$$\begin{aligned} x_k &= f_{k-1}(\hat{x}_{k-1}^+, 0) + \left.\frac{\partial f_{k-1}}{\partial x}\right|_{\hat{x}_{k-1}^+} (x_{k-1} - \hat{x}_{k-1}^+) + \left.\frac{\partial f_{k-1}}{\partial w}\right|_{\hat{x}_{k-1}^+} w_{k-1} \\ &= f_{k-1}(\hat{x}_{k-1}^+, 0) + F_{k-1}(x_{k-1} - \hat{x}_{k-1}^+) + L_{k-1} w_{k-1} \\ &= F_{k-1} x_{k-1} + [f_{k-1}(\hat{x}_{k-1}^+, 0) - F_{k-1}\hat{x}_{k-1}^+] + L_{k-1} w_{k-1} \\ &= F_{k-1} x_{k-1} + \tilde{w}_{k-1} \end{aligned} \tag{2.2}$$

Then, process noise $\tilde{w}_k$ can be defined as follows:

$$\tilde{w}_k \sim N\left(0, L_k Q_k L_k^T\right) \tag{2.3}$$

Similarly, linearizing the measurement model is as follows:

$$\begin{aligned} y_k &= h_k(\hat{x}_k^-, 0) + \left.\frac{\partial h_k}{\partial x}\right|_{\hat{x}_k^-} (x_k - \hat{x}_{k-1}^+) + \left.\frac{\partial h_k}{\partial v}\right|_{\hat{x}_k^-} v_k \\ &= h_k(\hat{x}_k^-, 0) + H_k(x_k - \hat{x}_k^-) + M_k v_k \\ &= H_k x_k + [h_k(\hat{x}_k^-, 0) - H_k \hat{x}_k^-] + M_k v_k \\ &= H_k x_k + z_k + \tilde{v}_k \end{aligned} \tag{2.4}$$

Then, z_k and measurement noise $\tilde{v}_k$ can be defined as follows:

$$z_k = h_k(\hat{x}_k^-, 0) - H_k\hat{x}_k^-$$
$$\tilde{v}_k \sim N\left(0, M_k R_k M_k^T\right) \tag{2.5}$$

The linearized system model of (2.2) and measurement model of (2.4) are obtained. Therefore, the state can be estimated using the standard Kalman filter equations. The following equations are for discrete-time EKF:

$$\begin{aligned} P_k^- &= F_{k-1}P_{k-1}^+F_{k-1}^T + L_{k-1}Q_{k-1}L_{k-1}^T \\ K_k &= P_k^- H_k^T\left(H_k P_k^- H_k^T + M_k R_k M_k^T\right)^{-1} \\ \hat{x}_k^- &= f_{k-1}(\hat{x}_{k-1}^+, w_{k-1}) \\ z_k &= h_k(\hat{x}_k^-, 0) - H_k\hat{x}_k^- \\ \hat{x}_k^+ &= \hat{x}_k^- + K_k(y_k - H_k\hat{x}_k^- - z_k) \\ &= \hat{x}_k^- + K_k(y_k - h_k(\hat{x}_k^-, 0)) \\ P_k^+ &= (I - K_k H_k)P_k^- \end{aligned} \tag{2.6}$$

2.2.3 INS-EKF-ZUPT

In IA-based PDR, to use ZUPT as a measurement, it is necessary to find a time interval when the shoe's speed becomes 0. At this time, this interval is called the stance phase. The shoe is attached to the ground during the stance phase, as shown in Figure 2.3.

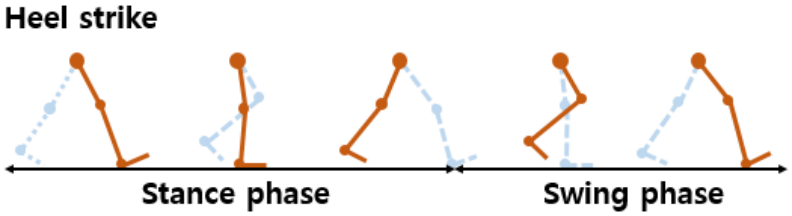

Figure 2.3: Phase classification during walking

During a normal gait, most of the magnitude of the acceleration measured by the foot-mounted IMU is composed of the pedestrian's moving direction and the direction perpendicular to the ground. Therefore, the acceleration signals in these two directions are used to detect the stance phase:

$$\begin{aligned} Energy &= \sqrt{a_x^2 + a_z^2} \\ Product &= a_x \cdot a_z \\ Sum &= a_x + a_z \end{aligned} \tag{2.7}$$

$$\begin{aligned} Condition_E &= \begin{cases} 1 & var(E_{k-l}: E_k) < th_E \\ 0 & otherwise \end{cases} \\ Condition_P &= \begin{cases} 1 & var(P_{k-l}: P_k) < th_P \\ 0 & otherwise \end{cases} \\ Condition_S &= \begin{cases} 1 & var(S_{k-l}: S_k) < th_S \\ 0 & otherwise \end{cases} \end{aligned} \tag{2.8}$$

where l is a window size. When all three conditions of (2.8) are 1, the stance phase is detected.

In IA-based PDR, the state of being estimated is as follows:

$$\delta x_k = \left[\delta p_k^n \ \vdots \ \delta v_k^n \ \vdots \ \delta\phi_k \ \delta\theta_k \ \vdots \ \delta\nabla_k^b\right] \tag{2.9}$$

where δp_k^n is position errors in the navigation frame, is velocity errors in the navigation frame, δv_k^n is north axis attitude error, $\delta\theta_k$ is east axis attitude error, and $\delta\nabla_k^b$ is accelerometer bias errors in the body frame.

The corresponding state transition matrix, Φ_k, is as follows:

$$\Phi_k = \begin{bmatrix} I_3 & I_3 \cdot \Delta t & O_{3\times2} & O_3 \\ O_3 & I_3 & S_{1,2}(f_k^n) \cdot \Delta t & \hat{\mathrm{C}}_b^n \cdot \Delta t \\ O_{2\times3} & O_{2\times3} & I_2 & O_{2\times3} \\ O_3 & O_3 & O_{3\times2} & I_3 \end{bmatrix} \tag{2.10}$$

where I and O are identity and zero matrices respectively, and the subscript below is the dimension of the matrix, Δt is time update period, $\hat{\mathrm{C}}_b^n$ is the estimate of rotation matrix from the body to navigation frame, f_k^n is the specific force in the navigation frame, and $S_{1,2}$ is the matrix with columns 1 and 2 of the skew-symmetric matrix.

Next, ZUPT, the measurement model, is described. ZUPT detects when the

foot's velocity reaches zero while it touches the ground and uses information that the speed of all three axes is zero. Thus, the observation matrix is shown in (2.11), and measurement updates are made during the stance phase shown in Figure 2.3:

$$H_k = [O_3 \quad I_3 \quad O_{3\times 2} \quad O_3] \tag{2.11}$$

In summary, the IA-based PDR system uses the system model to propagate the state variables in (2.9) with time update, and each time a stance phase is detected, it uses ZUPT as the measurement to correct them.

Chapter 3

Shape Analysis

The algorithm for classifying stair types by comparing the estimated walking direction will be introduced in Chapter 4 For this purpose, statistical shape analysis is used as a mathematical tool [21], described in this chapter. Here are some definitions that will be used in this chapter:

1. *The shape is defined as all the geometrical information that remains when location, scale, and rotational effects are removed from an object*.
2. *A landmark is defined as a point of correspondence on each object that matches between and within the population*.
3. *The configuration is defined as a set of landmarks on a particular object*.
4. *The configuration matrix X is the* $k \times m$ *matrix of Cartesian coordinates of the* k *landmarks in* m *dimensions*.
5. *The shape of a configuration matrix X is defined as all the geometrical information about X invariant under location, rotation, and isotropic scaling*.

Looking at the example shown in Figure 3.4, there are two '3' with the same shape in a 2-dimensional plane. There are ten landmarks in each of them. Therefore, the dimension of the configuration matrices is 10×2.

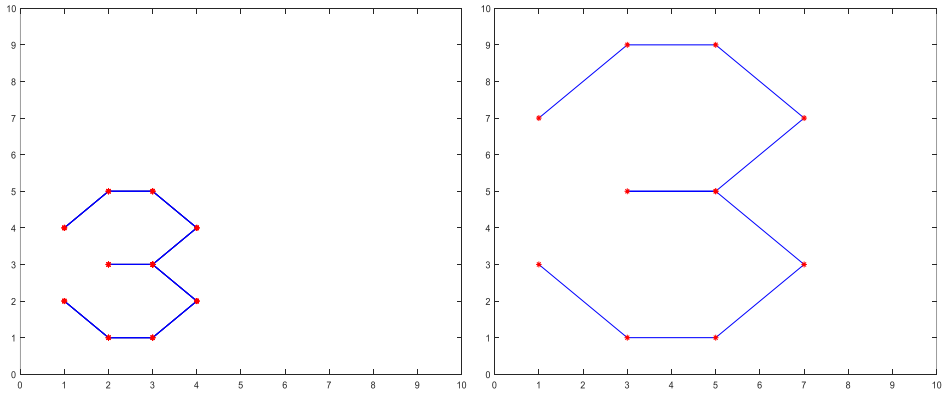

$$X = \begin{pmatrix} X_{(1)} \\ X_{(2)} \\ \vdots \\ X_{(10)} \end{pmatrix} = \begin{pmatrix} 1 & 2 \\ 2 & 1 \\ \vdots & \vdots \\ 1 & 4 \end{pmatrix} \qquad X = \begin{pmatrix} X_{(1)} \\ X_{(2)} \\ \vdots \\ X_{(10)} \end{pmatrix} = \begin{pmatrix} 1 & 3 \\ 2 & 1 \\ \vdots & \vdots \\ 1 & 7 \end{pmatrix}$$

(a) small '3' (b) large '3'

Figure 3.4: An example of landmark and configuration matrix

3.1 Euclidean Similarity Transformation

In this subchapter, a shape-maintaining transformation called Euclidean similarity transformation is introduced. The Euclidean similarity transformations of a configuration matrix X are described as follows:

$$\{\mu X\Gamma + \gamma : \mu \in \mathbb{R}^+, \Gamma \in SO(m), \gamma \in \mathbb{R}^m\} \tag{3.1}$$

where μ is the scale, Γ is a rotation matrix, and γ is a translation vector. This transformation can represent changes in scale, rotation, and translation while maintaining the overall shape of the feature represented by X. The two configuration matrices equal through the above transformations are defined as zero shape distances in shape analysis.

3.2 Full Procrustes Distance

First, a configuration matrix that represents the shape of a feature can be considered. Now, shape distance is a quantitative calculation of the morphological similarity between two configuration matrices, and the smaller the value, the more similar the shape of the two objects. The mathematical concept of this is described with some equations as follows.

The Helmert submatrix is introduced to eliminate the translation component of the configuration matrix. Equation (3.2) is the full Helmert matrix H^F with $k \times k$ dimension:

$$H^F = \begin{bmatrix} \frac{-1}{\sqrt{1\cdot 2}} & \frac{-1}{\sqrt{1\cdot 2}} & 0 & 0 & \cdots & 0 \\ \frac{-1}{\sqrt{2\cdot 3}} & \frac{-1}{\sqrt{2\cdot 3}} & \frac{-1}{\sqrt{2\cdot 3}} & 0 & \cdots & 0 \\ \vdots & \vdots & \vdots & \vdots & \vdots & \vdots \\ \frac{-1}{\sqrt{k(k+1)}} & \cdots & \cdots & \cdots & \cdots & \frac{-1}{\sqrt{k(k+1)}} \end{bmatrix} \tag{3.2}$$

The Helmert submatrix H is $(k-1) \times k$ matrix, the form of removing 1st row from (3.2). If H is multiplied by configuration matrix X, then HX is independent on the origin of X. In other words, H plays a role in removing the translation components. The form in which normalization is performed is then defined as pre-shape of a configuration matrix X, as shown in (3.3):

$$Z = HX/\|HX\| \tag{3.3}$$

where $\|-\|$ is Frobenius norm.

At last, the full Procrustes distance, the shape distance between the two configuration matrices, is defined. The full Procrustes distance d_F between X_1 and

X_2 is as follows:

$$d_F(X_1, X_2) = \inf_{\mu \in \mathbb{R}^+, \Gamma \in SO(m)} \|Z_2 - \mu Z_1 \Gamma\| \tag{3.4}$$

where $Z_r = HX_r / \|HX_r\|, r = 1,2$. The physical meaning of (3.4) is the minimum shape distance between X_1 and X_2 when X_1 is as close as possible to X_2 through the Euclidean similarity transformation. The analytic solution of the (3.4) exists as follows [21]:

$$d_F(X_1, X_2) = \sqrt{1 - tr(\Sigma)^2} \tag{3.5}$$

where $Z_r = HX_r / \|HX_r\|$, $r = 1,2$, $Z_2^T Z_1 = U \Sigma V^T$, $\hat{\Gamma} = VU^T$, and $\hat{\mu} = tr(\Sigma)$. Thus, the morphological similarity between the two features can be obtained, as shown in (3.5).

Chapter 4

Floor Determination

This chapter proposes an algorithm that classifies the types of stairs to determine the floor. The flow of this Chapter is as follows. First, the type of stairs considered in this study and a method based on shape analysis to identify the type of stairs are presented. Then, the concept of 'landing' is introduced to propose a floor determination algorithm using the stair type.

Before explaining the algorithm, the following assumptions are required in the algorithm.

1. *Pedestrians only use the stairs to move between floors. (excluding elevators)*
2. *Pedestrians do not change vertical direction while walking on stairs.*
3. *Stairs are classified into only the seven types set in Figure 4.5.*
4. *The stairs are connected one floor at a time. (e.g., stairs directly from the first floor to the third floor are not considered)*

4.1 Stair Types

This study claimed that different types of stairs could be distinguished through different shapes of walking direction signals. The stairs were grouped into seven types ($I, L, C, U, Square, \Delta, and\ Spiral$), as shown in Figure 4.5, which are common in general buildings [22]. Among them, I, L, C, and U can be grouped into cases with and without intermediate flatlands. However, the distinction between the two does not affect the classification of stair types or floors by introducing the 'landing' in this algorithm, and thus it is considered a class.

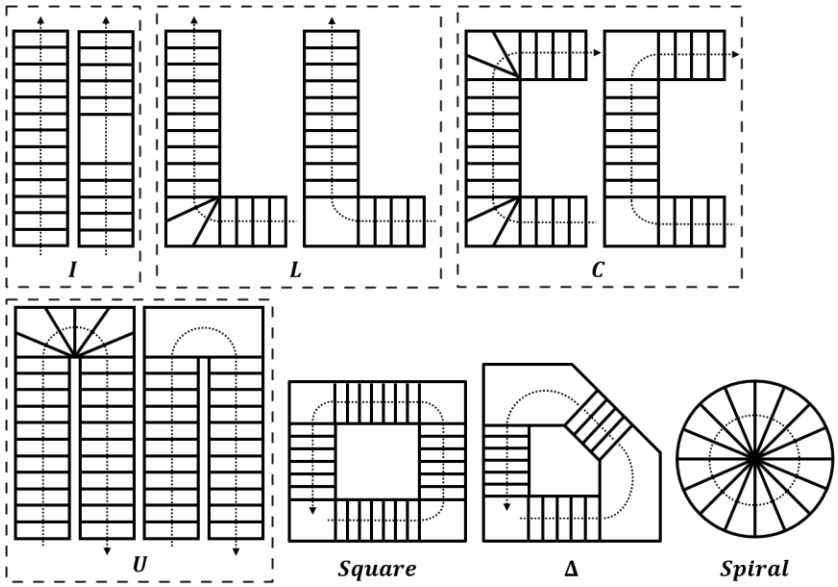

Figure 4.5: Stair types ($I, L, C, U, Square, \Delta, and\ Spiral$)

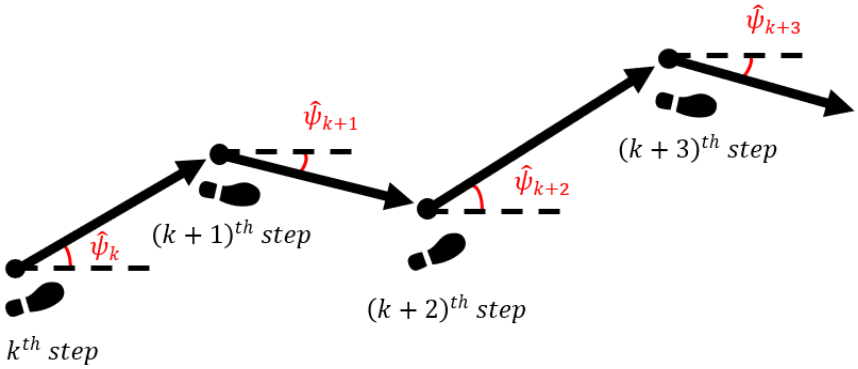

Figure 4.6: Walking direction when step is detected

4.2 Stair Type Classification Algorithm

Figure 4.6 shows how the walking direction is obtained. First, the estimated horizontal position in the PDR system is stored whenever a step is detected. The horizontal positions at the previous and current step detection are interconnected. Here, the direction of the vector is the walking direction. This algorithm sets the walking direction to 0° at the start of the stair walk. Thus, the walking direction starts at 0° regardless of the entrance direction of the staircase.

Now, how to classify stair types will be introduced by applying shape analysis in Chapter 2.2. First, the walking direction signal on stairs is generated for each of the seven stairs in Figure 4.5. This signal is called the nominal signal and is used as a reference. Next, walking direction signals obtained by simulating or experimenting with stair walking are called test signals. Here it can be inferred that the nominal and test signal shapes of the same type of stairs will be similar and thus will be distinguished from other types of stairs. Therefore, the shape distances between one test and seven nominal signals are calculated, and the stair type with the minimum value is determined, as shown in (4.1).

$$stair\ type = \underset{i=1\sim7}{\operatorname{argmin}} \left(d_F(\psi_{n,i}, \psi_t) \right), \tag{4.1}$$

where $\psi_{n,i}$ is i^{th} nominal walking direction signal of seven different stair types in Figure 4.5, and ψ_t is a test walking direction signal. It will be verified that stair types are well classified using (4.1) through simulations and experiments in Chapter 5

4.3 Floor Determination Algorithm

Figure 4.7 shows the overall floor determination algorithms. In Figure 4.7, $\hat{h}$ is the height estimated by the PDR system, and $\Delta\hat{h}_{k-1:k}$ represents the height change between the $(k-1)^{th}$ (prior) and the k^{th} (current) step detection time. This height change distinguishes flat land from stair walking. Then, the 'Stair type classification' is used to find the stair type through the walking direction signal described above. To classify the stair type, one set of the walking direction signal is needed, which appears in the sequential order of the walking direction. Therefore, there is a problem with knowing the starting and ending points of the walking direction signal. The start of the signal can be determined by '$\Delta\hat{h}_{k-1:k} > threshold$' in Figure 4.7. In addition, when moving through a single floor, it is easy to identify the end of the stair in the same way. However, in successive floor changes with repeated patterns, such as U type stairs, the stairs can be misclassified by tying them into one test signal set until more than two floors are changed rather than single. Therefore, the concept of 'landing' is defined as follows:

Definition: If the $\Delta\hat{h}$ between successive steps during stair, walking is less than *threshold1*, or $\Delta\hat{\psi}$ is greater than *threshold2*, it is defined as 'landing.'

In the above landing definition, the first condition is to distinguish the flat floor during stair walking, and the second condition is to detect a corner that changes direction during stair walking. Therefore, the presence or absence of intermediate flatlands of I, L, C, and U type stairs shown in Figure 4.5 does not require distinction because landing checks where the stairs change direction. Then, as shown in Figure 4.8, the stair type is classified each time landing occurs.

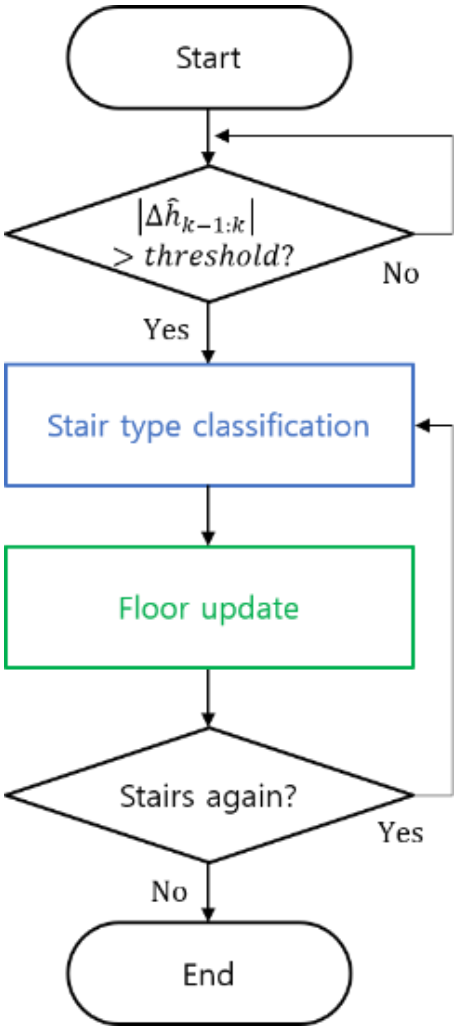

Figure 4.7: Floor determination algorithm (overall structure)

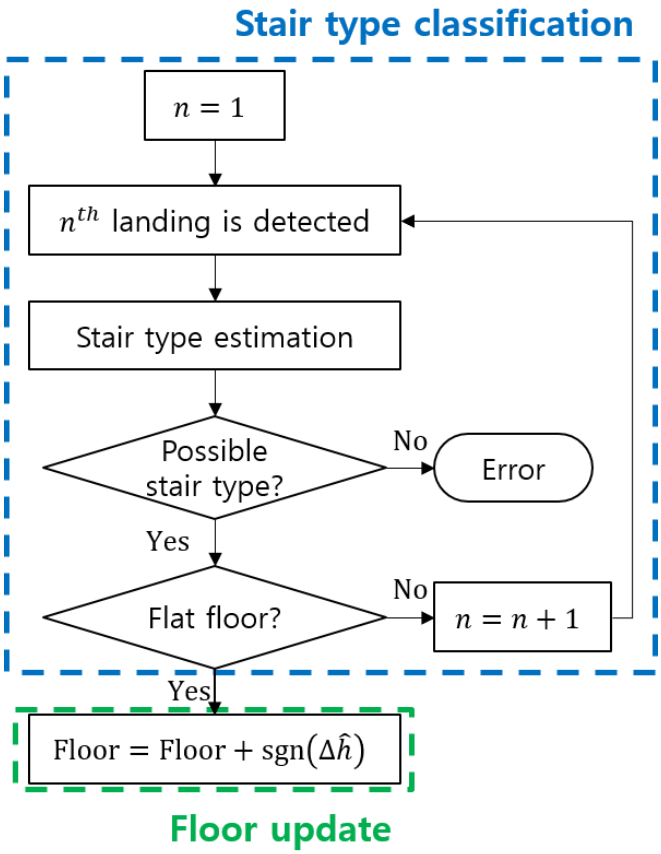

Figure 4.8: Floor determination algorithm (partial structure)

Table 4.1: Possible type of stair according to the number of landings

Numbers of landings	Possible stair type
1	$I, L, C, U, Square, \Delta, Spiral$
2	$L, C, U, Square, \Delta$
3	$C, Square, \Delta$
4	$Square$

In Figure 4.8, 'Possible stair type' is the type of stairs that can come out when n^{th} landing is detected and is associated with the number of corners in the staircase. Table 4.1 shows the possible stair type depending on the number of landings. For example, the 2^{nd} landing is detected, and an L or U type stair is classified. However, this may be the end of an L or U type stair, but it may be detected in the mid-flat corner of C, Δ, or $Square$ type stairs. Therefore, as shown in Figure 4.8, the' Flat floor' condition is introduced to distinguish this ambiguity. This condition determines the walking of flat land, not stairs, after landing occurs. In this algorithm, the 'Flat floor' condition is applied if the difference between the maximum and minimum values of $\hat{h}$ for three steps immediately after landing is less than the threshold. Using the window for three steps is to distinguish it from the intermediate flat land. If this condition is not applied, the stair type has not yet been determined, so the 'Stair type classification' loop will continue, but the stair type will be classified if applied. It then detects the floor change and changes the floor according to the sign of $\Delta\hat{h}$, the total change of height through the 'Floor update.'

Thus, the floor is well determined immediately after the stair walk ends. Furthermore, the proposed algorithm does not require additional sensors, infrastructure, or assumptions about floor height. Therefore, this study is also applicable to buildings with different floor heights.

Chapter 5

Simulation and Experimental Results

This Chapter consists of three sub-chapters: simulations (Chapter 5.1), single-floor change experiments (Chapter 5.2), and multi-floors change experiments (Chapter 5.3). First, Chapter 5.1 shows that the stair type can be classified by the shape of the walking direction signal. Next, Chapter 5.2 verifies that stair types are well distinguished when changing a single floor. Finally, in Chapter 5.3, experimental scenarios that move multiple floors are designed, including two or more stair types, and it is ensured that the stair type determination algorithm described in Chapter 5 works well. In addition, this study identifies that problems arising from conventional methods are resolved using the proposed algorithm.

5.1 Simulation Results

Before proceeding with the simulation, a nominal signal is needed as a reference. The nominal walking direction signals considering the shape of the seven stairs in Figure 4.5 are shown in Figure 5.1.

Nominal signals are ideal and appear in a straight line, as they represent the constant speed of stair walking without noise. When deriving the experimental results in Chapters 4.2 and 4.3, the above nominal signals are used again as a reference.

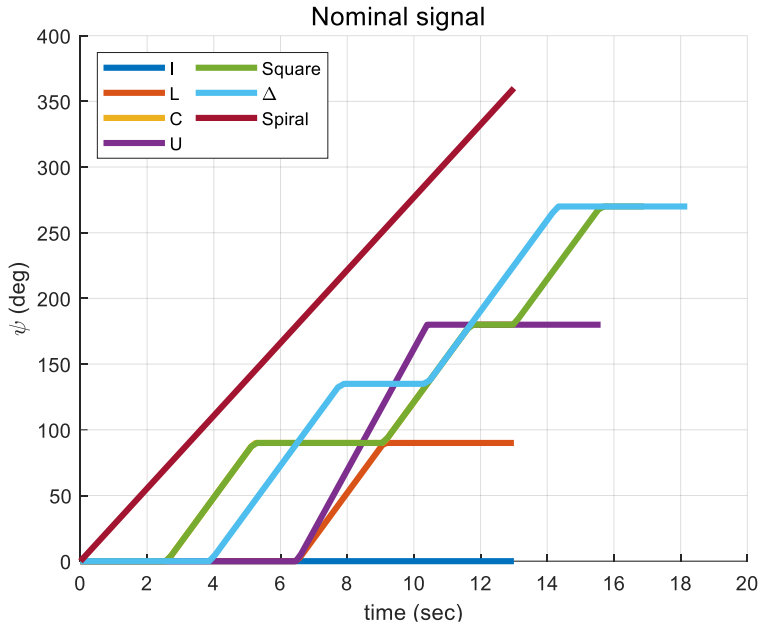

Figure 5.1: Nominal signal of walking direction

Table 5.1: Simulation conditions obtained from experiments

Simulation conditions	
$\mu_{\Delta t}$	1.3 sec
$\sigma_{\Delta t}$	0.11 sec
$\mu_{\Delta \psi}$	0°
$\sigma_{\Delta \psi}$	2.5°

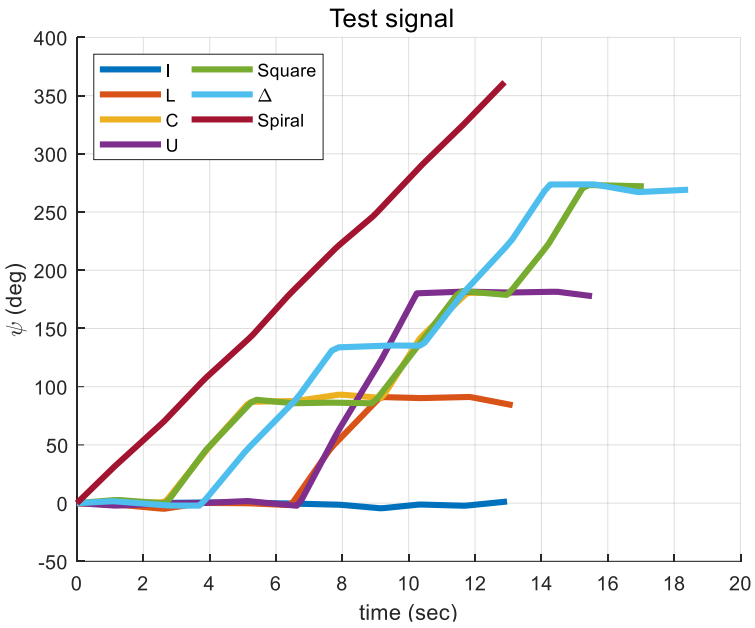

Figure 5.2: Test signal from simulation (all types)

Unlike nominal signals, test signals should be similar to the actual walking direction of pedestrians. When walking on stairs, the walking direction signals appear in a form that contains noise, not a straight line, as shown in Figure 5.1. Therefore, to consider this noise, the average values of several experiments were obtained through stair walk experiments and summarized in Table 5.1.

In Table 5.1, Δt means the period of step detection based on the right foot. $\sigma_{\Delta t}$ is a standard deviation of the step detection period, which is considered because pedestrians' walking speed is not constant. And $\sigma_{\Delta\psi}$ is the standard deviation of walking direction estimated through the PDR system, which is considered because zigzag walking directions signal due to human behavior characteristics, or inaccuracies in attitude estimated in the PDR system may affect the error factors. A test signal is made considering the values corresponding to Table 5.1, and the results are shown in Figure 5.3. Figure 5.3 seems to be similar to the nominal signal in

Figure 5.1, but the test signals come in a non-straight line because of the error factors considered.

Single floor movement experiments were conducted on five stair types $(I, L, C, U, and\ \Delta)$ to verify that the walking direction signals by stair types generated in the above simulation are similar in real-world experiments. Figure 5.3 and Figure 5.4 show the walking direction signals obtained from simulation and experiments for each stair type.

Comparing Figure 5.3 and Figure 5.4, the signals made by simulation and experiments have similar shapes for the same type of stairs. Therefore, in real-world experiments, it can also be expected that stair types can be classified with walking direction signals, and this is confirmed in Chapter 5.2. Next, pre-shape is obtained by normalizing it as in (6) before calculating the shape distance between the nominal and test signals, as shown in Figure 5.5.

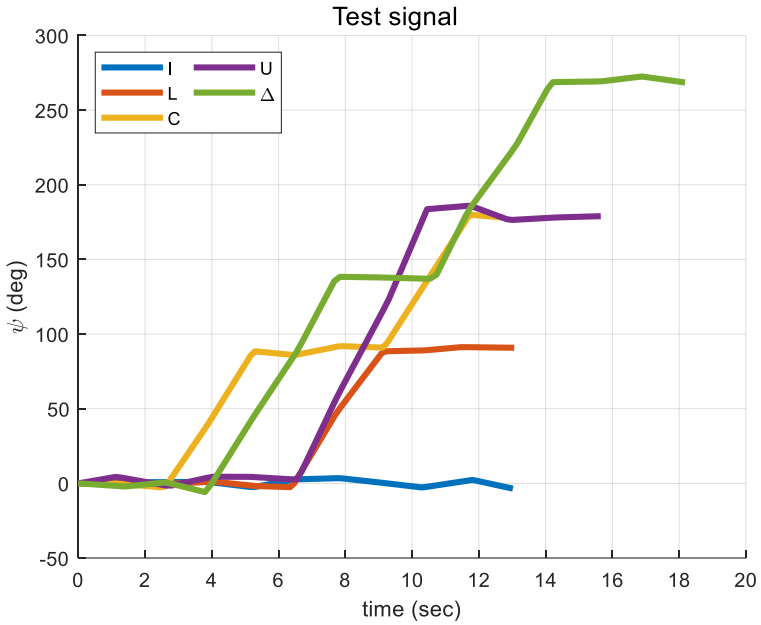

Figure 5.3: Test signal from simulation (5 types)

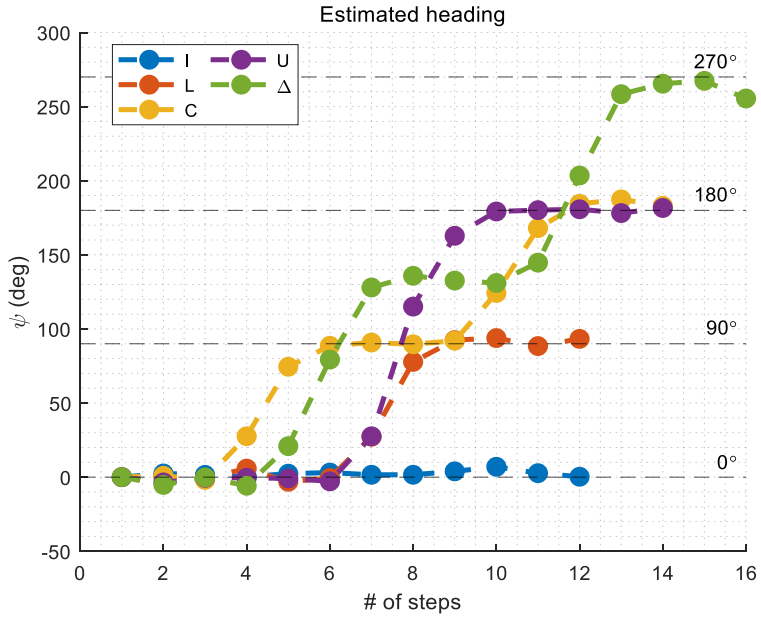

Figure 5.4: Test signal from an experiment (5 types)

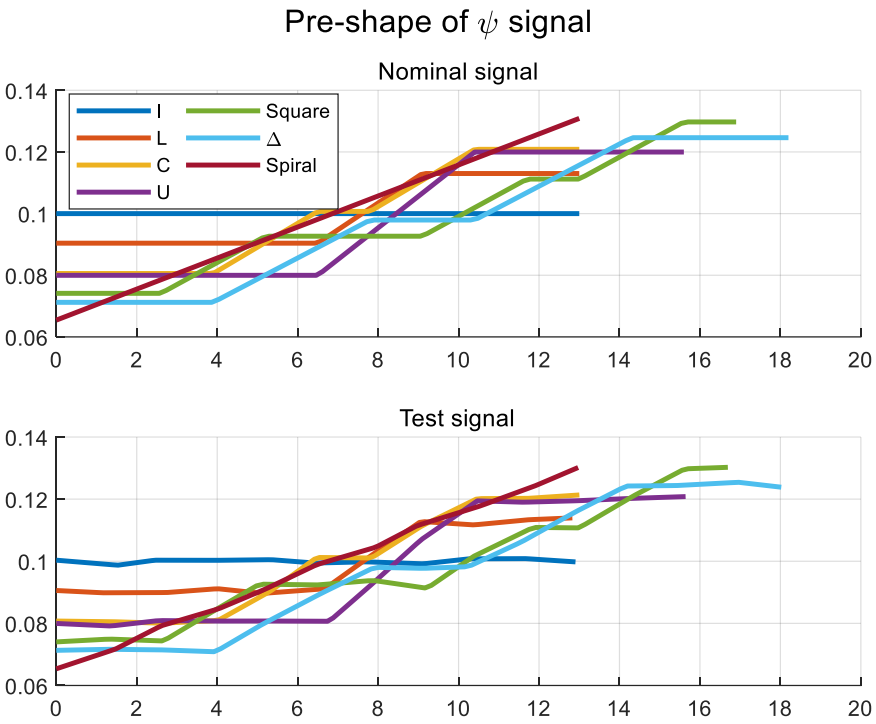

Figure 5.5: Pre-shape of nominal and test signal

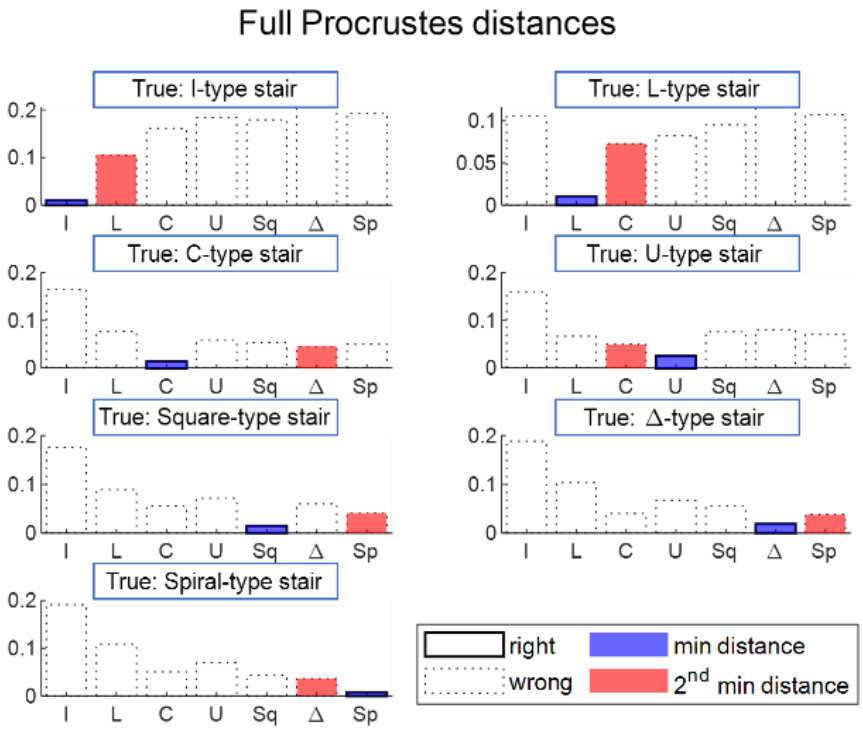

Figure 5.6: Classification results of each test signal by finding minimum shape distance (simulation)

Now, the shape distances of each test signal and the nominal signals are obtained and shown in Figure 5.6.

Figure 5.6 shows that both the actual stair type and the stair type estimated by shape distance as the minimum (blue) are consistent. It also shows the stair type with the second smallest shape distance (red), clearly distinguished from the blue with the smallest shape distance in magnitude.

The accuracy was verified through Monte-Carlo simulation because random noise was mixed when test signals were generated. A total of 70,000 Monte-Carlo simulations were conducted, and the results are shown in Table 5.2. In Table 5.2, all 70,000 times, stair types are accurately identified without misdetection.

Table 5.2: Results of 70,000 Monte-Carlo simulations with original simulation conditions

		Output							
	# / %	*I*	*L*	*C*	*U*	*Square*	Δ	*Spiral*	Accuracy
Target	*I*	10000 100	0 0	0 0	0 0	0 0	0 0	0 0	10000 100
	L	0 0	10000 100	0 0	0 0	0 0	0 0	0 0	10000 100
	C	0 0	0 0	10000 100	0 0	0 0	0 0	0 0	10000 100
	U	0 0	0 0	0 0	10000 100	0 0	0 0	0 0	10000 100
	Square	0 0	0 0	0 0	0 0	10000 100	0 0	0 0	10000 100
	Δ	0 0	0 0	0 0	0 0	0 0	10000 100	0 0	10000 100
	Spiral	0 0	0 0	0 0	0 0	0 0	0 0	10000 100	10000 100
	F1-score	10000 1.0000	10000 1.0000	10000 1.0000	10000 1.0000	10000 1.0000	10000 1.0000	10000 1.0000	70000 100

Table 5.3: Results of 70,000 Monte-Carlo simulations with new simulation conditions

		Output							
	# / %	*I*	*L*	*C*	*U*	*Square*	Δ	*Spiral*	Accuracy
Target	*I*	10000 100	0 0	0 0	0 0	0 0	0 0	0 0	10000 100
	L	145 1.45	9797 97.97	58 0.58	0 0	0 0	0 0	0 0	10000 97.97
	C	0 0	89 0.89	9910 99.10	0 0	0 0	0 0	1 0.01	10000 99.10
	U	0 0	0 0	0 0	10000 100	0 0	0 0	0 0	10000 100
	Square	0 0	0 0	0 0	0 0	10000 100	0 0	0 0	10000 100
	Δ	0 0	0 0	0 0	0 0	0 0	10000 100	0 0	10000 100
	Spiral	0 0	0 0	0 0	0 0	0 0	0 0	10000 100	10000 100
	F1-score	10145 0.9928	9886 0.9853	9968 0.9926	10000 1.0000	10000 1.0000	10000 1.0000	10001 1.0000	70000 99.58

In addition, to check the robustness of this algorithm, the value of the $\sigma_{\Delta t}$ and $\sigma_{\Delta \psi}$ in Table 5.1 was doubled, and the walking direction offset error was also added. A walk can cause the walking direction offset error in an oblique direction in the stair or by an error factor such as incorrect gyro bias estimation, and the 1-sigma value is set to 15°, generating randomly at each corner of the stairs. These newly considered errors will reduce the similarity between the test and nominal signal, and the algorithm's robustness can be checked. Similarly, 70,000 Monte-Carlo simulation results with new simulation conditions are summarized in Table 5.3. Unlike previous results in Table 5.2, stair type misdetection occurred but was less frequent, and still, some stair types were classified as 100% accurate.

However, if the 1-sigma value of the walking direction offset error was set below 10° instead of 15°, the accuracy was 100%, as shown in Table 5.2.

5.2 Experimental Results – Single Floor Change

Figure 5.7: Foot mounted IMU used in experiments

The experiments were conducted by attaching IMU on the right side of the shoe, as shown in Figure 5.7. A single-floor change experiment was conducted on five stair types $(I, L, C, U, and\ \Delta)$, and the corresponding walking direction signals are shown in Figure 5.4. Similar to simulations in Chapter 5.1, after converting the walking

direction signals in Figure 5.4 to pre-shapes, the shape distances with the nominal signals are obtained and summarized in Figure 5.8.

Figure 5.8 shows that both the actual stair type and the stair type estimated by shape distance as the minimum (blue) are consistent. Thus, like the simulation results, the stair types could be classified well through the walking direction signals in experiments.

As a result of the experiment, stairs of type I or L are clearly distinguished from other stair types. However, the remaining five stair types have relatively minor differences from the second minimum distance compared to I and L. So, the additional experiments were conducted for each type of stair three times up and three times down, and in all trials, the stair types were accurately classified, as shown in Figure 5.8.

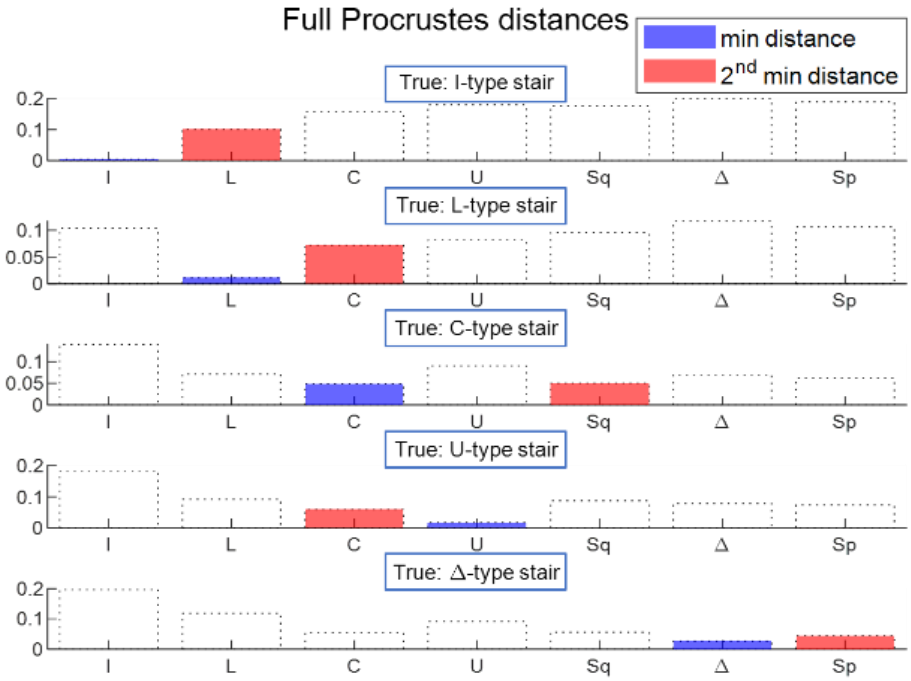

Figure 5.8: Classification results of each test signal by finding minimum shape distance (experiment)

5.3 Experimental Results – Multiple Floor Changes

Next, Chapter 5.3 presents the results of floor determination with the proposed algorithm through experiments moving through multiple floors. In order to prove the validity of the proposed algorithm, not only would it be necessary to classify the stair types well but also to determine the floors accurately. Therefore, the experiments were conducted in two scenarios, three times each.

5.3.1 Scenario – 1

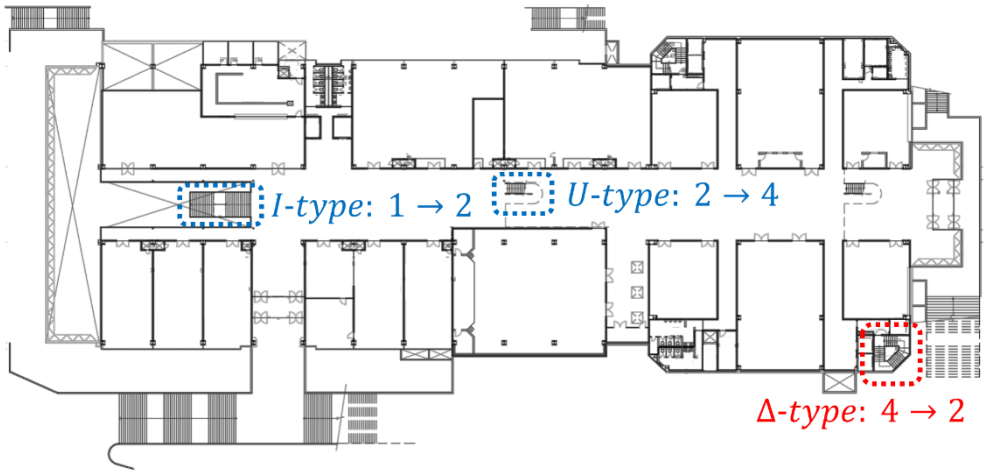

Figure 5.9: Floor plan of Scenario 1 building

Table 5.4: Floor changes and corresponding stair types in Scenario 1

Floor change	Stair type
1 → 2	*I*
2 → 3	*U*
3 → 4	*U*
4 → 3	Δ
3 → 2	Δ

The floor moved in Scenario 1 and the type of stairs used are shown in Table 5.4, and Figure 5.9 is a floor plan of the experimental building. What is unique about the building in Scenario 1 is that the first floor is about 70cm higher than the other floors. In addition, the I type stair used to move from the first to the second floor contains intermediate flat land.

The stair type and floor determination results obtained from the proposed algorithm are shown in Figure 5.10.

In Figure 5.10 (a), five stair walks were detected, and the classified stair types from each detection appeared in order of $I - U - U - \Delta - \Delta$. This is consistent with the type of stairs that walked. So, even when moving through multiple floors like this, the type of stairs is well distinguished through algorithms in Figure 4.7.

In Figure 5.10 (b), the results of the floor determination are shown with the estimated height (red dot). Different floors are shaded with different colors. As a result, there was a slight time delay, but it was confirmed that the floors were accurately determined. Therefore, this algorithm classifies stair types and provides floor determination results well.

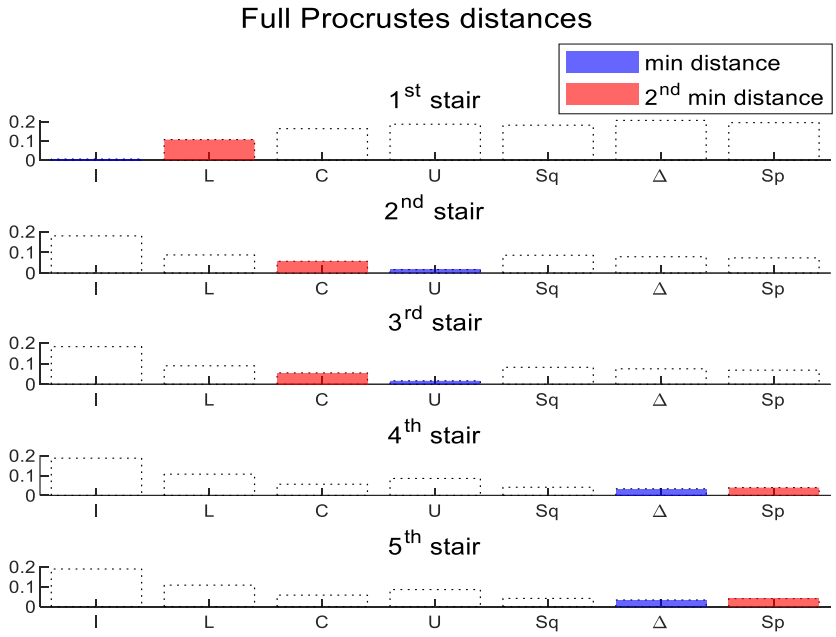

(a) Stair type classification results

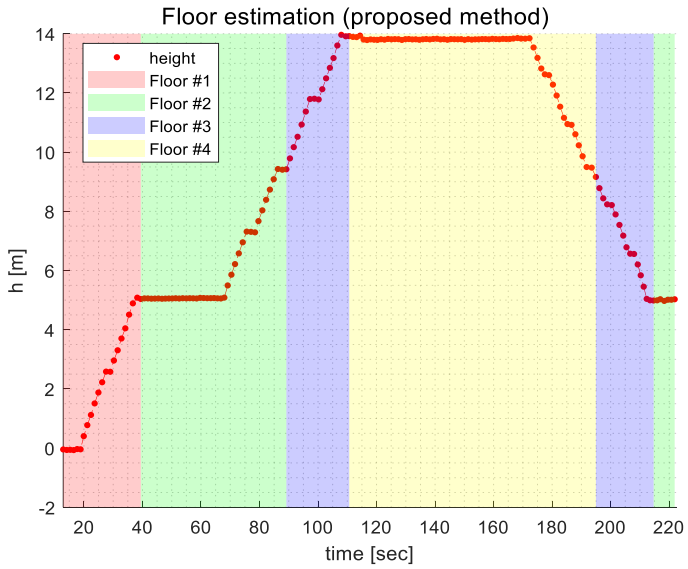

(b) Floor determination results by the proposed method

Figure 5.10: Experimental results of Scenario 1 with the proposed method

Next, the results are compared by applying a conventional method of determining floors by assuming floor height for the same experimental data. As a building typically has a floor height of around 4m, this method was applied assuming the floor height of 3.9m and 4.1m, respectively, and the results were shown in Figure 5.11.

In Figure 5.11 (a), assuming the height of the floor was 3.9 m, it was incorrectly calculated from the fourth floor to the fifth. This is caused by the fact that the height of the first floor is higher than that of other floors. In addition, even if all the floors have the same height, incorrect thresholds can lead to miscalculations when moving through multiple floors. In Figure 5.11 (b), which is a result of assuming a floor height of 4.1 m, the order of floor change was correct ($1 \rightarrow 2 \rightarrow 3 \rightarrow 4 \rightarrow 3 \rightarrow 2$), but the problem remains that the timing of floor change is not valid. In other words, the actual floor change is very different from the floor change using the conventional method. For example, according to this method, the floor will be changed from the second floor to the third floor in 70 seconds, which is closer to the second floor. On the other hand, the floor changes from the fourth floor to the third floor in 190 seconds, but it goes down to the second floor after passing the third floor. Thus, when floors are determined using this method, the floor may be miscalculated due to improper thresholds when moving through multiple floors, and the timing of floor determination is unclear.

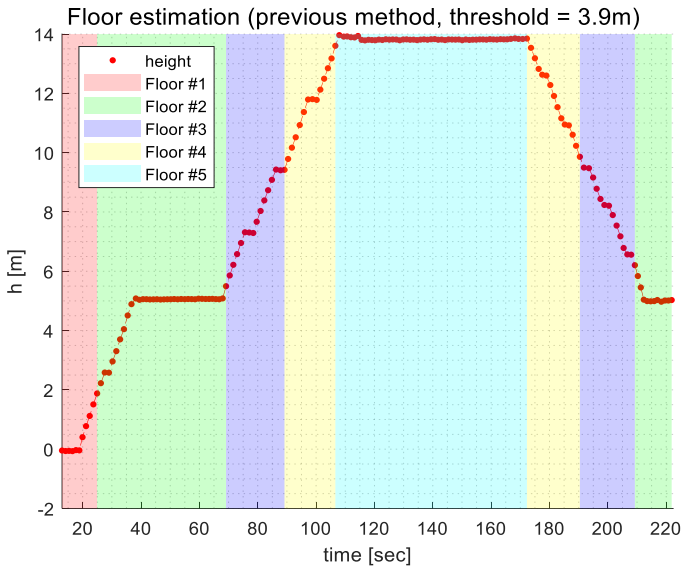

(a) Floor determination results (floor height=3.9m)

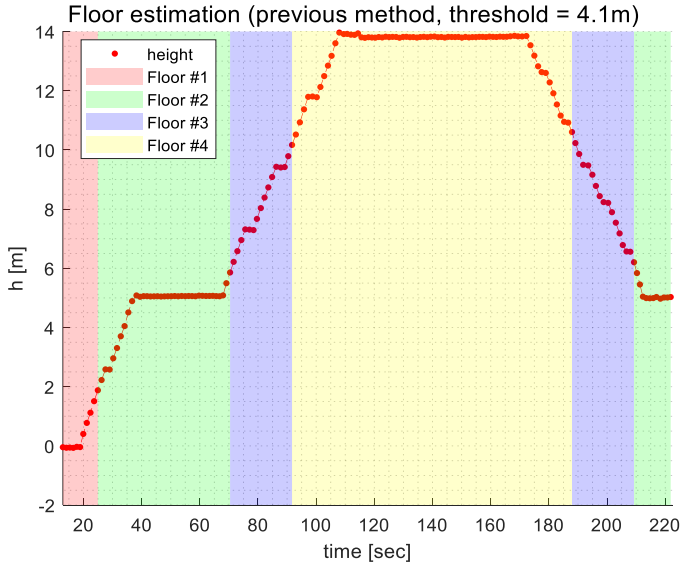

(b) Floor determination results (floor height=4.1m)

Figure 5.11: Experimental results of Scenario 1 with the conventional method

5.3.2 Scenario – 2

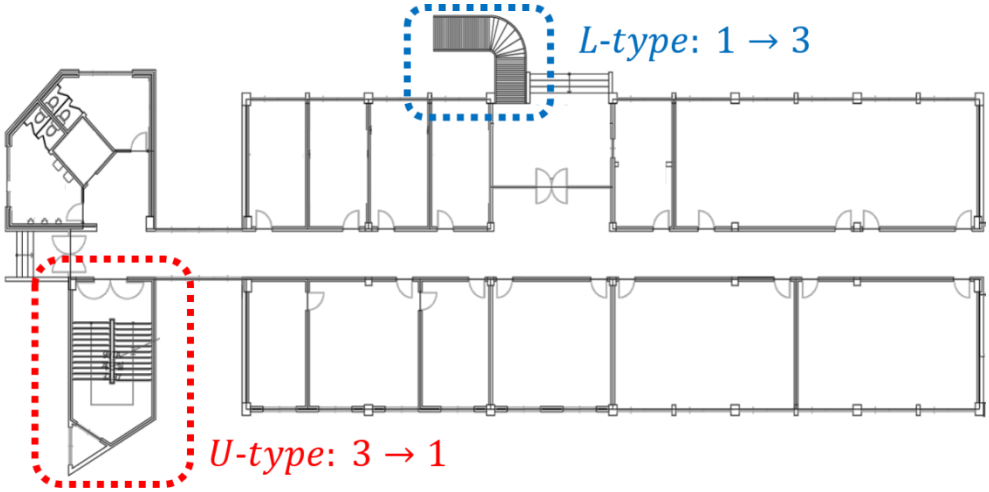

Figure 5.12: Floor plan of Scenario 2 building

Table 5.5: Floor changes and corresponding stair types in Scenario 2

Floor change	Stair type
1 → 2	*L*
2 → 3	*L*
3 → 2	*U*
2 → 1	*U*

The floor moved in Scenario 2 and the type of stairs used are shown in Table 5.5, and Figure 5.12 is a floor plan of the experimental building. In Scenario 2, even on the same first floor, there is a special note that the heights at the entrance of the L type stairs and the U type stairs are different.

As in Scenario 1, the experimental results are summarized in Figure 5.13. In Figure 5.13 (a), four stair walks were detected, and the estimated stair types from each detection appeared in order of $L-L-U-U$. Furthermore, the shaded Chapter in Figure 5.13 (b) shows that the floors are accurately determined

immediately after the floor changes. Thus, in Scenario 2, as in Scenario 1, the proposed algorithm identifies the exact determination of stair types and floor changes.

There is another way of using a barometer concerning floor determination [23]. However, this pressure altitude could not be used alone to determine the floors, and the floor determination algorithm should be used together. However, there is no need to use additional sensors or infrastructures inside the building in our proposed method. Moreover, even if the height of each floor is different, the floors can be determined well without the floor height assumption.

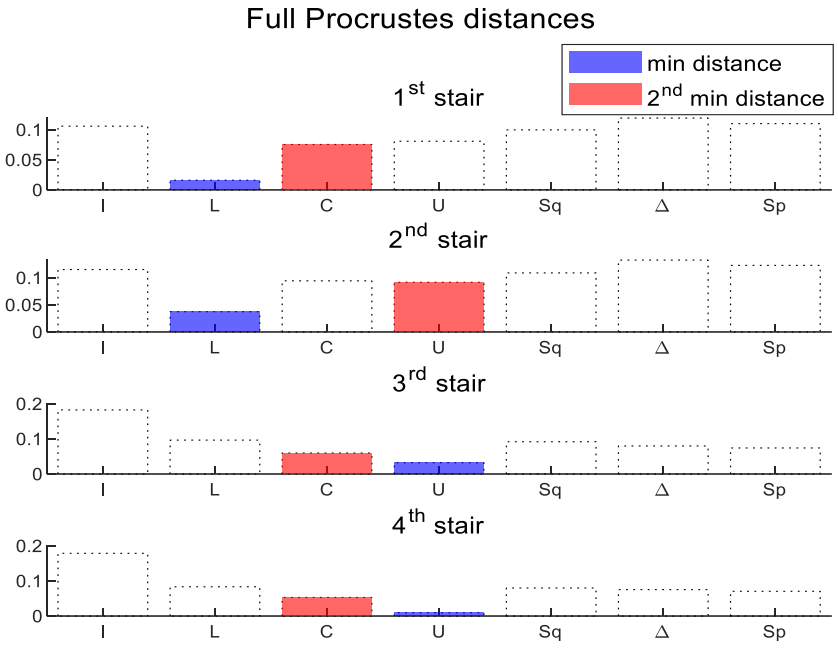

(a) Stair type classification results

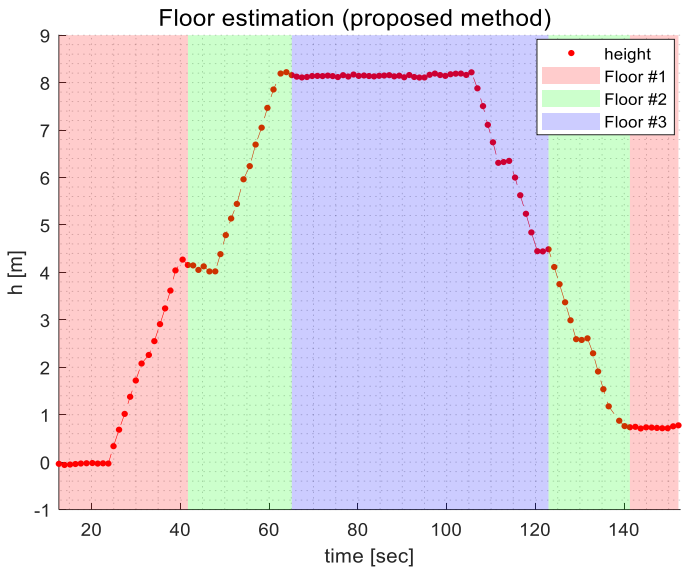

(b) Floor determination results by the proposed method

Figure 5.13: Experimental results of Scenario 2 with the proposed method

Chapter 6

Conclusion

6.1 Conclusion and Summary

This thesis proposed a new floor determination algorithm based on walking direction signal shape from the PDR system using MEMS IMU. Stairs were grouped into seven types: I, L, C, U, $Square$, Δ, and $Spiral$, and these are distinguishable by different shapes of walking direction signal. Thus, shape analysis was used to classify the stair types as a mathematical tool.

As the first step to apply shape analysis, the reference walking direction signals, called nominal signals, are generated. Next, the test signals were acquired through simulations and experiments. Then, the Full Procrustes distances between nominal and test signals were calculated to find a stair type with minimum shape distance. With estimated stair type, 'landing' and 'possible stair type' introduced in Chapter 4 were implemented to determine floor using the algorithm in Figure 4.7.

The proposed algorithm was verified through simulations and experiments. Both simulation and experiment classification results matched the actual stair types. Next, two experimental scenarios are designed with multiple floor changes and stair types, where our algorithm showed improved performance in determining the floors compared to the conventional method. Therefore, our algorithm can accurately determine floors without using wireless infrastructures, additional sensors, or any

prior knowledge on buildings such as floor height.

6.2 Future Work

To apply the proposed algorithm, some assumptions were made at the beginning of Chapter 4. For example, errors may occur if the direction is changed while going up the stairs, stairs other than the classified seven stairs are used, or if one stair connects several floors at once. Chapter 4.3 also introduced the concept of 'landing' to determine floors. 'Landing' means a corner in the stairs or a point to reach flat ground, and it is identified by comparing the magnitude with the threshold for $\Delta\hat{h}$ or $\Delta\hat{\psi}$, respectively. Therefore, there is a problem determining this threshold, and the value may vary depending on the pedestrian or walking environment. Therefore, if this point can be improved and applied to more general situations, the algorithm's robustness will increase.

This study was applied to an IA-based PDR system using a foot-mounted IMU. The reason is that the stability of the step detection algorithm and the accuracy of the walking direction required in this study are relatively higher in IA than in PA. However, PA is more valuable because it can be applied to smartphones because the inertial sensor has fewer positional restrictions. Therefore, if the step detection algorithm and heading estimation accuracy in PA are improved, this study can be applied to PA too.

Bibliography

[1] L. Mainetti, L. Patrono and I. Sergi, "A Survey on Indoor Positioning Systems," *Proceedings of the 22nd International Conference on Software, Telecommunications and Computer Networks (SoftCOM)*, Split, Croatia, pp. 111–120, September 2014.

[2] N. Fallah, I. Apostolopoulos, K. Bekris, and E. Folmer, "Indoor Human Navigation Systems: a Survey," *Interacting with Computers*, vol. 25, no. 1, pp. 21–33, 2013.

[3] L. M. Ni, Y. Liu, Y. C. Lau, and A. P. Patil, "LANDMARC: Indoor Location Sensing Using Active RFID," *Proceedings of the 1st IEEE International Conference on Pervasive Computing and Communications (PerCom 2003)*, Fort Worth, Texas, USA, pp. 407–415, March 2003.

[4] Y. Gu, A. Lo, and I. Niemegeers, "A Survey of Indoor Positioning Systems for Wireless Personal Networks," *IEEE Communincations Surveys & Tutorials*, vol. 11, no. 1, pp. 13–32, 2009.

[5] J. Baus, A. Kruger, and W. Wahlster, "A Resource-Adaptive Mobile Navigation System," *Proceedings of the 7th International Conference on Intelligent User Interfaces*, San Francisco, California, USA, pp. 15–22, 2002.

[6] L. Ran, S. Helal, and S. Moore, "Drishti: An Integrated Indoor/Outdoor Blind Navigation System and Service," *Proceedings of the 2nd IEEE Annual Conference on Pervasive Computing and Communications (PerCom 2004)*, Orlando, Florida, USA, pp. 23–30, March 2004.

[7] K. Lorincz, and M. Welsh, “MoteTrack: A Robust, Decentralized Approach to RF-based Location Tracking,” *Personal and Ubiquitous Computing*, vol. 11, no. 6, pp. 489–503, 2007.

[8] J. Hightower and G. Borriello, “Location Systems for Ubiquitous Computing,” *IEEE Computer Society*, vol. 34, no. 8, pp. 57–66, August 2001.

[9] P. Prasithsangaree, P. Krishnamurthi, and P. K. Chrysanthis, “On Indoor Position Location with Wireless LANs,” *Proceedings of the 13rd IEEE International Symposium on Personal, Indoor and Mobile Radio Communications*, Lisbon, Portugal, vol. 2, pp. 720–724, September 2002.

[10] H. Ju, M. S. Lee, S. Y. Park, J. W. Song, and C. G. Park, “A Pedestrian Dead-Reckoning System That Considers the Heel-Strike and Toe-off Phases when Using a Foot-mounted IMU,” *Measurement Science and Technology*, vol. 27, no. 1, Art. no. 015702, 2015.

[11] J. W. Kim, H. J. Jang, D. H. Hwang, and C. Park, “A Step, Stride and Heading Determination for the Pedestrian Navigation System,” *Journal of Global Positioning Systems*, vol. 3, no. 1–2, pp. 273–279, 2004.

[12] J. Parviainen, J. Kantola and J. Collin, “Differential Barometry in Personal Navigation,” *2008 IEEE/ION Position, Location and Navigation Symposium*, Monterey, California, USA, pp. 148–152, 2008.

[13] K. Itzik and L. Yaakov, “Step-Length Estimation During Movement on Stairs,” *2019 27th Mediterranean Conference on Control and Automation (MED)*, Akko, Israel, pp. 518–523, July 2019.

[14] D. C. Song, J. H. Lee, S. Park, and C. G. Park, “Walking Condition Awareness Algorithm Using Barometer in Smartphone for Pedestrian

Navigation," *2020 IPNT, The Institute of Positioning, Navigation and Timing*, Yeosu, Korea, November 2020.

[15] S. L. Ting, S. K. Kwok, A. H. Tsang, and G. T. Ho, "The Study on Using Passive RFID Tags for Indoor Positioning," *International Journal of Engineering Business Management*, vol. 3, no.1, pp. 9–15, 2011.

[16] Widyawan, M. Klepal and D. Pesch, "Influence of Predicted and Measured Fingerprint on the Accuracy of RSSI-based Indoor Location Systems," *2007 4th Workshop on Positioning, Navigation and Communication*, Hannover, Germany, pp. 145–151, 2007.

[17] F. Alsehly, T. Arslan, and Z. Sevak, "Indoor Positioning with Floor Determination in Multi-Story Buildings," *2011 International Conference on Indoor Positioning and Indoor Navigation*, Guimaraes, Portugal, pp. 1–7, 2011.

[18] Y. Gu, M. Ma, Y. Li and Q. Song, "Accurate Height Estimation Based on Apriori Knowledge of Buildings," *International Conference on Indoor Positioning and Indoor Navigation*, Montbéliard, France pp. 1–7, 2013.

[19] S. Boim, G. Even-Tzur and I. Klein, "Height Difference Determination Using Smartphones Based Accelerometers," *IEEE Sensors Journal*, 2021.

[20] S. Y. Cho, J. H. Lee, and C. G. Park, "Stable Zero-Velocity Detection Method Regardless of Walking Speed for Foot-mounted PDR," *Journal of Positioning, Navigation, and Timing*, vol. 9, no. 1, pp. 33–42, 2020.

[21] I. L. Dryden, "Statistical Shape Analysis," Wiley StatsRef: Statistics Reference Online, 2014.

[22] S. Y. Park, M. S. Lee, H. Ju, and C. G. Park, "Floor Classification Algorithm Based on Stair Awareness Using MEMS IMU," *Proceedings of the 27th*

International Technical Meeting of the Satellite Division of The Institute of Navigation (ION GNSS+ 2014), Tampa, Florida, USA, pp. 1616-1621, September 2014.

[23] J. Luo, C. Zhang, and C. Wang, "Indoor Multi-floor 3D Target Tracking Based on the Multi-sensor Fusion," *IEEE Access*, vol. 8, pp. 36836–36846, 2020.

[24] D. Kim, Y. Lee, and C. G. Park, "Context Awareness and Step Length Estimation by Shape Distance and H-features," *International Journal of Control, Automation, and Systems*, vol. 18, pp. 3051–3061, 2020.

국문초록

본 논문에서는 관성 측정 장치(IMU: Inertial Measurement Unit)를 이용한 실내 보행자 항법에서 계단을 통한 층 이동 시 계단의 종류를 파악하여 층을 결정하는 새로운 알고리즘을 제안한다. 이를 위해 보행자항법(PDR: Pedestrian Dead Reckoning) 시스템에서 추정된 고도, 걸음 검출 시간, 그리고 방향각을 사용한다. 이때 추정된 고도는 계단 보행을 시작하거나 마칠 때 평지 보행과 구분될 정도의 정확도만 필요하다. 따라서 본 알고리즘에서는 기존의 층 구분 알고리즘에서 필요로 하는 고도 추정치에 대한 의존성을 최소화할 수 있다. 제안한 알고리즘에서는 계단 보행 시에 나타나는 방향각의 신호에 통계적 형상 분석(statistical shape analysis) 기법을 적용하여 계단의 종류를 파악한 후 층을 구분하게 된다. 시뮬레이션과 실험을 통해 제안한 알고리즘의 정확도를 검증하며 여러 종류의 계단을 여러 층 오르내리는 경우에도 알고리즘이 잘 동작함을 확인한다. 그리고 기존의 층 구분 알고리즘에서 발생하는 시간 지연 문제를 해결하고 층 구분 정확도가 높아진 것을 확인한다. 또한 본 연구는 관성 측정장치 이외의 다른 센서나 무선통신 장치를 사용하지 않으며 층 높이와 같은 건물에 대한 기본 정보를 가정하지 않고도 층을 잘 결정할 수 있다는 유효성을 가진다.

주요어: 보행자항법시스템, 실내 항법, 층 구분, 통계적 형상 분석, 형상 거리, 분류 알고리즘

학번: 2020-20377